

Corrosion Performance of Different Aluminum Alloy Deposits Fabricated by Lateral Friction Surfacing

William A. Relue*, Ebrahim Seidi, L.H. Hihara, Scott F. Miller

Department of Mechanical Engineering, University of Hawaii at Manoa
Honolulu, Hawaii, USA

*Email: wrelue@hawaii.edu

Abstract

Friction surfacing technique is a thermo-mechanical approach for metallic deposition, suitable for a broad range of materials and applications. Friction surfacing can be employed for various industrial purposes such as coating, welding, repairing defective parts, surface hardening, and improving corrosion performance. In this technique, frictional heat generated at the interface of the consumable tool and substrate results in a severe plastic deformation at the end of the rod, enabling the deposition of a consumable material on the substrate surface.

In this investigation, a novel method in friction surfacing, lateral friction surfacing, is employed to deposit the aluminum coatings. In this novel approach, the side of the consumable tool is pressed against the surface of the substrate, and the material transfer happens from the lateral surface of the tool. This technique provides extremely thin and smooth deposits, which are more consistent compared to the conventional approach of friction surfacing. Moreover, this technique enables fabricating of deposits in lower temperatures, lessening the thermal impacts on the microstructures and mechanical properties of the deposits.

In this investigation plates of 1018 mild steel were partially coated with various aluminum alloys and corroded in an accelerated corrosion test chamber. The corrosion performance of the partially coated sample was evaluated by mass loss measurement. It was found that AA5086 offered the most corrosion protection. After 13 cycles of GM9540P test, equivalent to approximately 3½ years exposure at a mild/moderate marine site in Hawaii, almost all of the deposited aluminum was consumed.

Keywords: *Corrosion, Friction Deposition, Multilayer Coating, Side of the Tool, Solid-State deposition*

1. Introduction

Friction surfacing (FS) technique is a friction-based additive manufacturing approach for metallic deposition, suitable for a broad range of tool/substrate material combinations and applications [1]. Friction surfacing can be employed for various industrial purposes such as coating, welding, repairing defective parts, surface hardening, and improving corrosion performance of surfaces. In this approach, frictional heat developed at the tool/substrate interface results in severe plastic deformation of the tool material, enabling the deposition of a consumable material on the substrate surface [1].

Friction surfacing is a thermo-mechanical approach resulting in a friction deposition that depends on several critical process parameters with a high level of complexity. Several attempts have been made to study the relationship between the process parameters and the coating quality and geometry. Several attempts have already been made by the researchers to determine the influence of important process factors such as the forging force [2-5], traverse speed [4-6], and spindle speed [2-7] on the coating quality. Several investigations have focused on different combinations of tool/substrate material for the consumable rod and workpiece, however, majority of these investigations are focused on aluminum and steels [8]. Furthermore, there are several studies on employing reinforcing particles in order to improve the coating quality [9-13]. For this purpose, holes with different configurations along the length of the rod should be created to provide enough space for inserting the reinforcing particles.

A novel method in friction surfacing entitled lateral friction surfacing was employed to deposit extremely thin and smooth coating layers by forging the radial surface of the consumable rod onto the workpiece [14, 15]. This technique provides the deposition in lower process temperatures compared to the friction deposition from the end of the tool. This study is an attempt to investigate the corrosion performance of the coatings deposited through the lateral friction surfacing technique by evaluating the mass loss after accelerated corrosion test.

A few studies [16-18] have done investigations concerning the corrosion performance of friction surfaced materials in consideration of the corrosion potential, potentiodynamic polarization, electrochemical impedance spectroscopy (EIS), and various immersion techniques; however, the studies have not have used GM9540P accelerated corrosion test as a means to evaluate corrosion performance.

The GM9540 test is an accelerated corrosion test standardized by General Motors in the late 1990's to give the capability to quickly and repeatably corrode any given sample to a desired level of corrosion. At its

most fundamental level, the test takes advantage of the synergistic effects of temperature and surface chemistry to rapidly accelerate the rate of corrosion a component might experience in the field. Originally, this test was not well known. However, in the early 90's a research group from the Society of Automotive engineers produced a study evaluating several accelerated corrosion techniques, and found that an earlier version of the GM9540P was the most effective at predicting cosmetic corrosion of cold rolled steels. As a result, this technique garnered more popularity and attention as a method to evaluate materials for their corrosion properties. One cycle of this test has three parts. The first being called the "soak" where the sample is sprayed multiple times with the salt solution for about 30 seconds over the course of 8 hours. Second is the "wet heat" where the humidity is controlled and elevated to 100% RH. The temperature is held constant at 49 C for the duration of this 8 hour period. Lastly, is the "hot dry off" which consists of a ramp up of the temperature to 60 C and held for the remainder of this 8 hour period. Humidity is maintained at less than 30% RH for the last portion of the hot dry off period as illustrated in Figure xx. [19].

In the comparison of the corrosivity of the GM9540P test to that encountered in natural environments, one cycle of the GM9540P was equivalent to approximately 100 days of exposure to a mild marine environment for 1008 plain carbon steel (Coconut Island (CI), Kaneohe Bay, Oahu) [20]. The environmental parameters for CI were temperature (26.2°C), relative humidity (76.5%), chloride deposition rate (51.3 mg/m²/day), and time of wetness (14 %) [20]. The 1018 plain carbon steel samples in this investigation were exposed for 13 cycles in the GM 9540P test, corresponding to approximately 3 1/2 years of exposure to CI, a mild/moderate marine site based on the 1008 plain-carbon steel data.

2. Materials and Methods

In this study, the lateral friction surfaced deposits of five different aluminum alloys, AA1100, AA2024, AA5086, AA6061, and AA7075, were fabricated on the surface of AISI 1018 carbon steel substrates by utilizing a customized JET JMD-18 milling machine, as shown in Fig. 1. The *physical properties and chemical composition of these materials are presented in Tables 1-6 [21]*. In order to fabricate the coatings, the constant spindle speed of 2300 rpm and traverse speed of 76.2 mm/min were employed, while the pressing force of 150 N was applied and controlled manually by means of a Kistler 9272 drilling dynamometer and LabVIEW programming. The deposition process was conducted in a way that two passes of deposit were fabricated in one track to provide a better coating coverage. The consumable aluminum rods with a diameter of 12.7 mm and the length of 100 mm, and the steel substrates with the dimensions of 127mm × 63.5mm × 6.35mm were utilized.

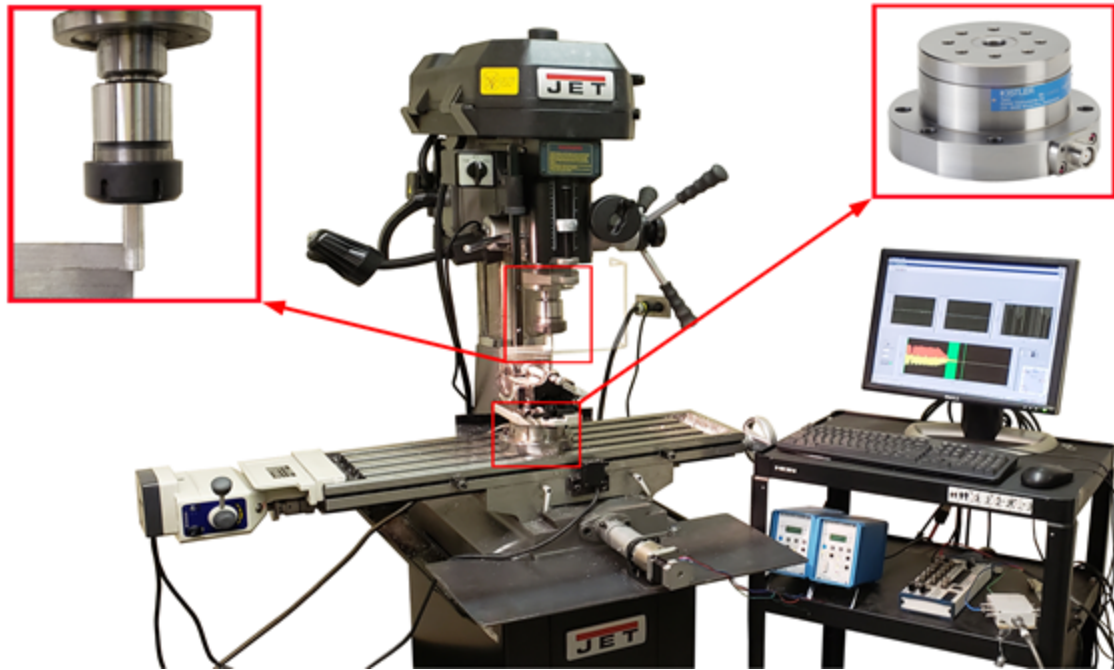


FIGURE1. The customized JET JMD-18 milling machine equipped with a dynamometer and data acquisition system [14]

Table 1. Chemical composition and physical properties of AA1100-O

<i>Elements</i>	<i>Mg</i>	<i>Cr</i>	<i>Mn</i>	<i>Zn</i>	<i>Si+Fe</i>	<i>Al</i>
% of composition	0.050	0.04-0.35	0.05	0.10	0.95	Balance
<i>Physical Property</i>	<i>Melting Point</i>	<i>UTS</i>	<i>Elongation at Break</i>		<i>Thermal Conductivity</i>	
Values	643 - 657.2 °C	89.6 MPa	25%		222 W/m.K	

Table 2. Chemical composition and physical properties of AA2024-T4

<i>Elements</i>	<i>Mg</i>	<i>Si</i>	<i>Cu</i>	<i>Cr</i>	<i>Mn</i>	<i>Ti</i>	<i>Zn</i>	<i>Fe</i>	<i>Al</i>
% of composition	0.8-1.2	0.4-0.8	0.15-0.4	0.04-0.3 5	0.15	0.15	0.25	0.7	Balance

Physical Property	Melting Point	UTS	Elongation at Break	Thermal Conductivity
Values	502-638°C	395 MPa	8.0 - 12% @ 24.0°C	121 W/m.K

Table 3. Chemical composition and physical properties of AA5086-H32

Elements	Mg	Si	Cu	Cr	Mn	Ti	Zn	Fe	Al
% of composition	3.5 - 4.5	0.4	0.10	0.05 - 0.25	0.20 - 0.70	0.15	0.25	0.50	Balance
Physical Property	Melting Point	UTS	Elongation at Break	Thermal Conductivity					
Values	585.0-640.6 °C	290 MPa	6-12% @ 24.0°C	125 W/m.K					

Table 4. Chemical composition and physical properties of AA6061-T6

Elements	Mg	Si	Cu	Cr	Mn	Ti	Zn	Fe	Al
% of composition	0.8-1.2	0.4-0.8	0.15-0.4	0.04-0.35	0.15	0.15	0.25	0.7	Balance
Physical Property	Melting Point	UTS	Elongation at Break	Thermal Conductivity					
Values	588°C	310 MPa	17% @ 24.0°C	167 W/m.K					

Table 5. Chemical composition and physical properties of AA7075-T6

Elements	Mg	Si	Cu	Cr	Mn	Ti	Zn	Fe	Al
% of composition	2.1-2.9	0.4	1.2-2	0.18-0.28	0.3	0.2	5.1-6.1	0.5	Balance
Physical Property	Melting Point	UTS	Elongation at Break	Thermal Conductivity					
Values	477°C	572 MPa	11% @ 24.0°C	130 W/m.K					

Table 6. Chemical composition of AISI 1018 low carbon steel

Elements	Mn	P	S	C	Fe
----------	----	---	---	---	----

% of composition	0.60 - 0.90	≤ 0.040	≤ 0.050	0.14 - 0.20	98.81 - 99.26
Physical Property	Melting Point	UTS	Elongation at Break	Thermal Conductivity	
Values	1480°C	440 MPa	15 % @ 24.0°C	51.9 W/mK	

	AA1100	AA2024	AA5086	AA6061	AA7075	1018 Steel
Main Alloying Element(s)	Si + Fe	Mg + Si + Fe	Mg	Mg + Si + Fe	Mg + Zn	Mn
Melting Point	643-657.2	502-638	585-641	588	477	1480
UTS (MPa)	89.6	395	290	310	572	440
Elongation (% @ 24 C)	25	10	9	17	11	15
Thermal Conductivity W/m.K	222	121	125	167	130	51.9

Preparation for exposure in the CCTC consisted of a brief 5 minute sonication in a 0.1% liquinox solution followed by a rinse with methanol to remove any remaining grease or machine oils.

Modified GM9540 Accelerated Corrosion Test

A Singleton Cyclic Corrosion Test Chamber (CCTC) was used to subject samples to a modified GM9540 accelerated corrosion test (Figure X) , using a salt mist solution that consisted of 0.9% sodium chloride, 0.1% calcium chloride and 0.25% sodium bicarbonate. The samples were exposed to 13 day cycles. In a standard GM9540P test, the normal of the sample face would be tilted no more than 15 degrees from the horizontal. However, in this study the samples were tilted 60 degrees from the horizontal as shown in figure xx.

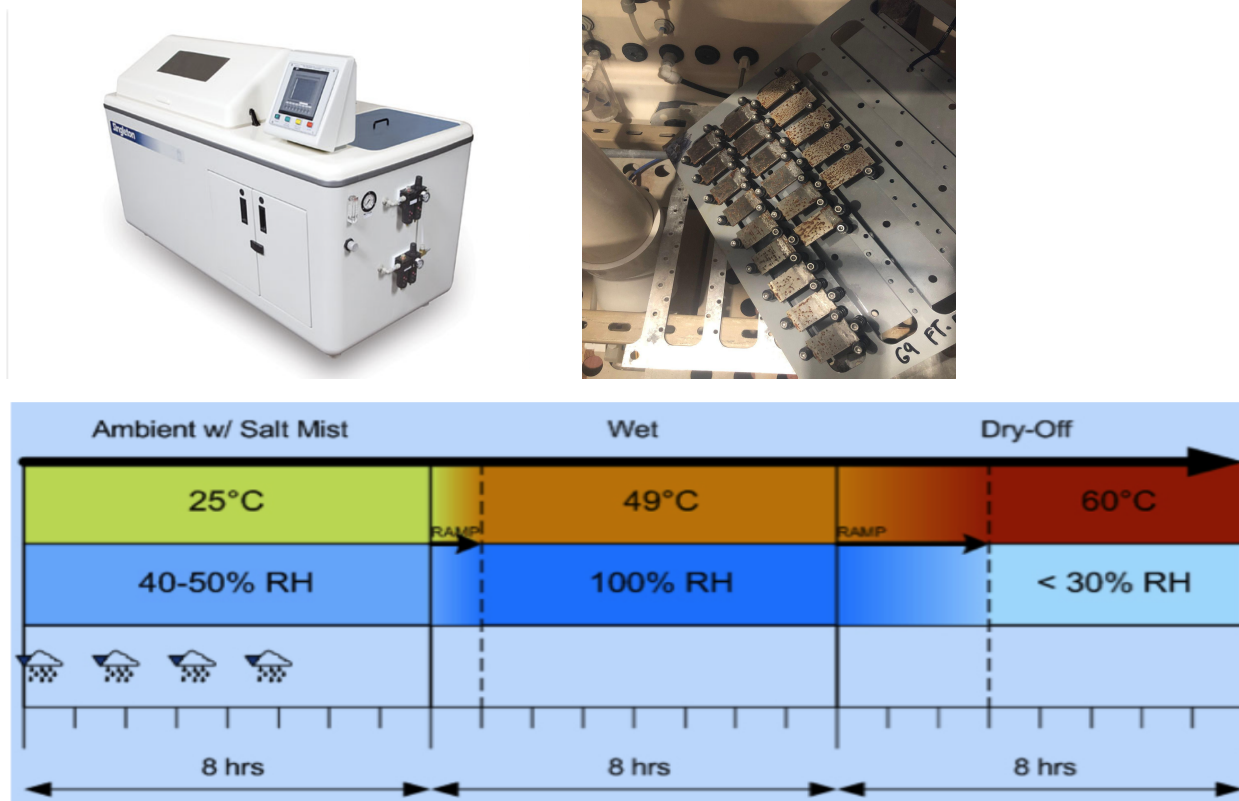


Figure xx. The CCTC chamber and an illustration of one cycle in the chamber. Image courtesy from Daniel P. Schmidt, USA AMC

After corrosion in the CCTC, the corrosion product was removed by glass bead blasting. The glass bead blasting removed the corrosion products, remaining aluminum coating, but not the 1018 substrate steel. Once the plate samples showed an off-white matte color, they were considered “cleaned”. The samples were then rinsed with methanol and dried. After drying the weight was taken by a Mettler Toledo XP504 scale.

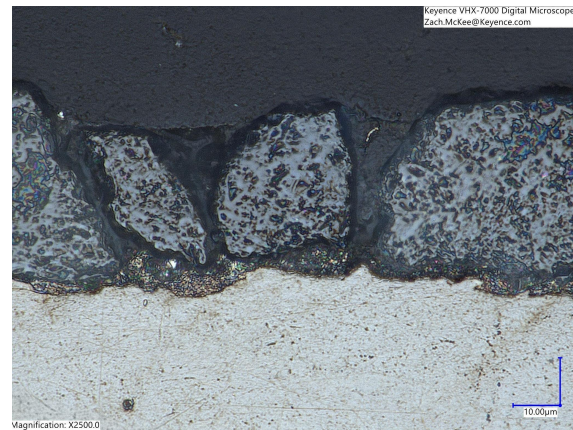
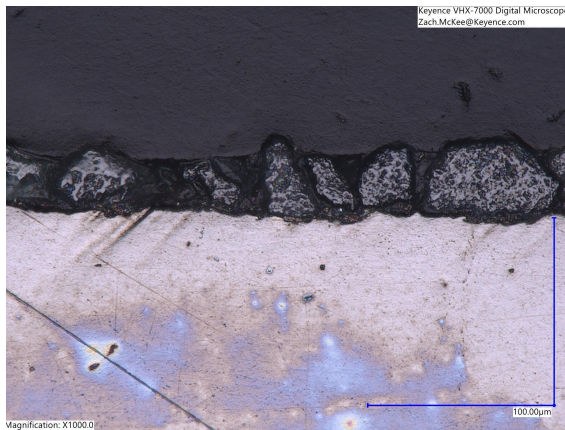
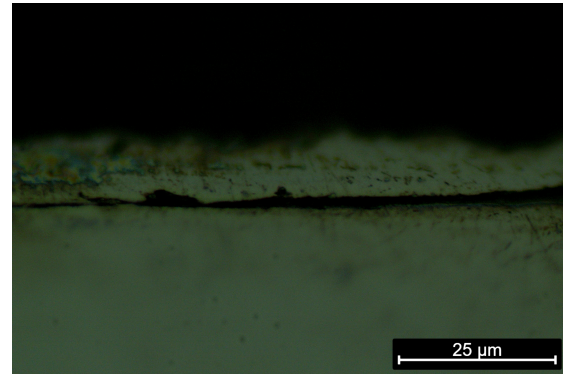
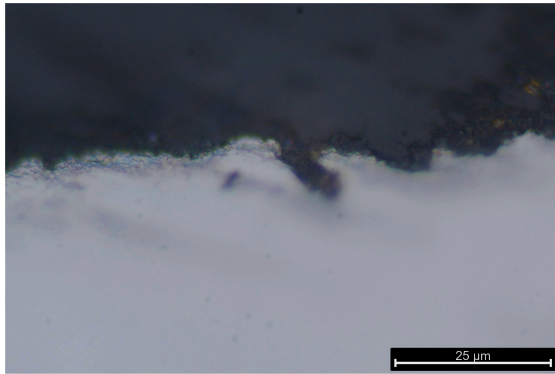
The average penetration rate was determined from weight loss measurements, exposed surface area, and duration in the CCTC. Since the coupons were deposited on precision ground 2”-wide 1018 steel bar, and then cut into 1” sections, the original mass of the 1018 coupons was estimated by calculating the volume of the 1018 substrate and multiplying by the measured density. The dimensions of each coupon was measured to 0.01 mm precision.

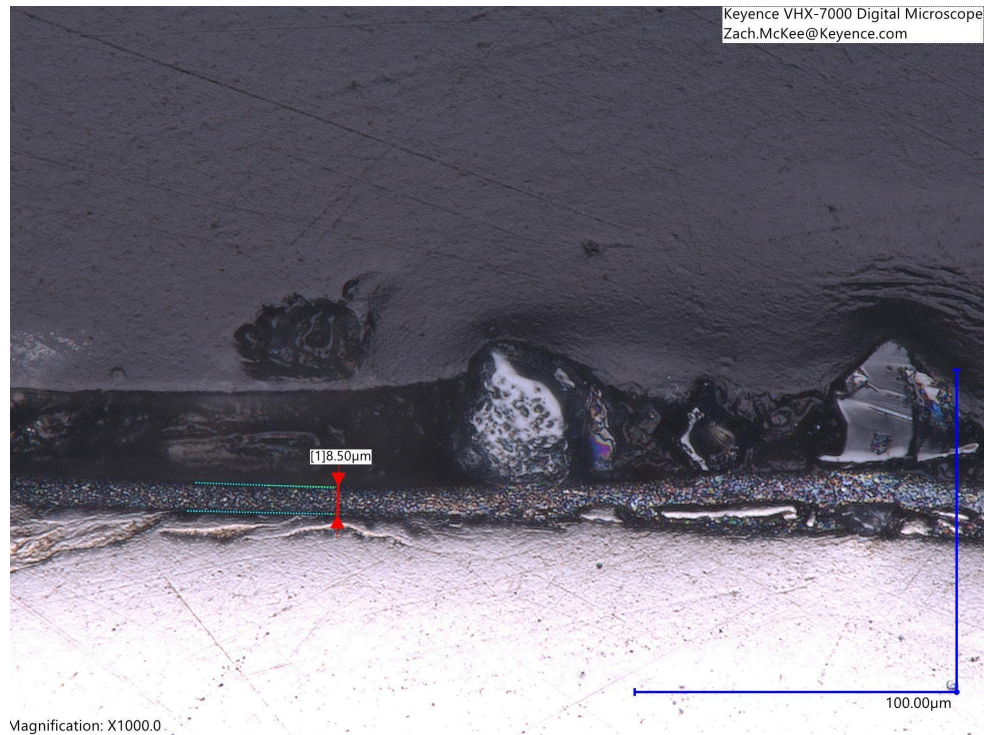
Surface work function was measured at the boundary between aluminum and steel from a top-down view by Scanning Kelvin Probe technique. The work function (ϕ) is a measure of how much energy is required to displace an electron from the surface of a metal. The work function can vary between materials.

3. Results and Discussion





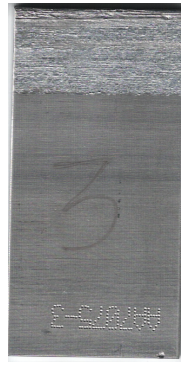

Coatings

The visual images of the aluminum coatings (Figure 1a) indicated that the coatings were not totally continuous. Some regions of the coatings had textured or flaky appearance. In addition, the amount of deposited aluminum was not consistent on all of the surfaces. For example, there were some AA5086 coatings with a thick discontinuous deposit (Figure 1a). Some regions of a AA6061 sample showed a thin continuous layer (Keyence photo) and regions with an appearance of an aggregated layer (Keyence photo).





In Figure 1, a typical sample from each group is shown. By visual inspection, it was apparent that AA5086 offered the longest lasting corrosion protection for not only the coated region, but some areas outside as well. This was confirmed in the mass loss measurements presented in Figure 2.

Condition	AA1100	AA2024	AA5086	AA6061	AA7075	Blank
Virgin (3a)						

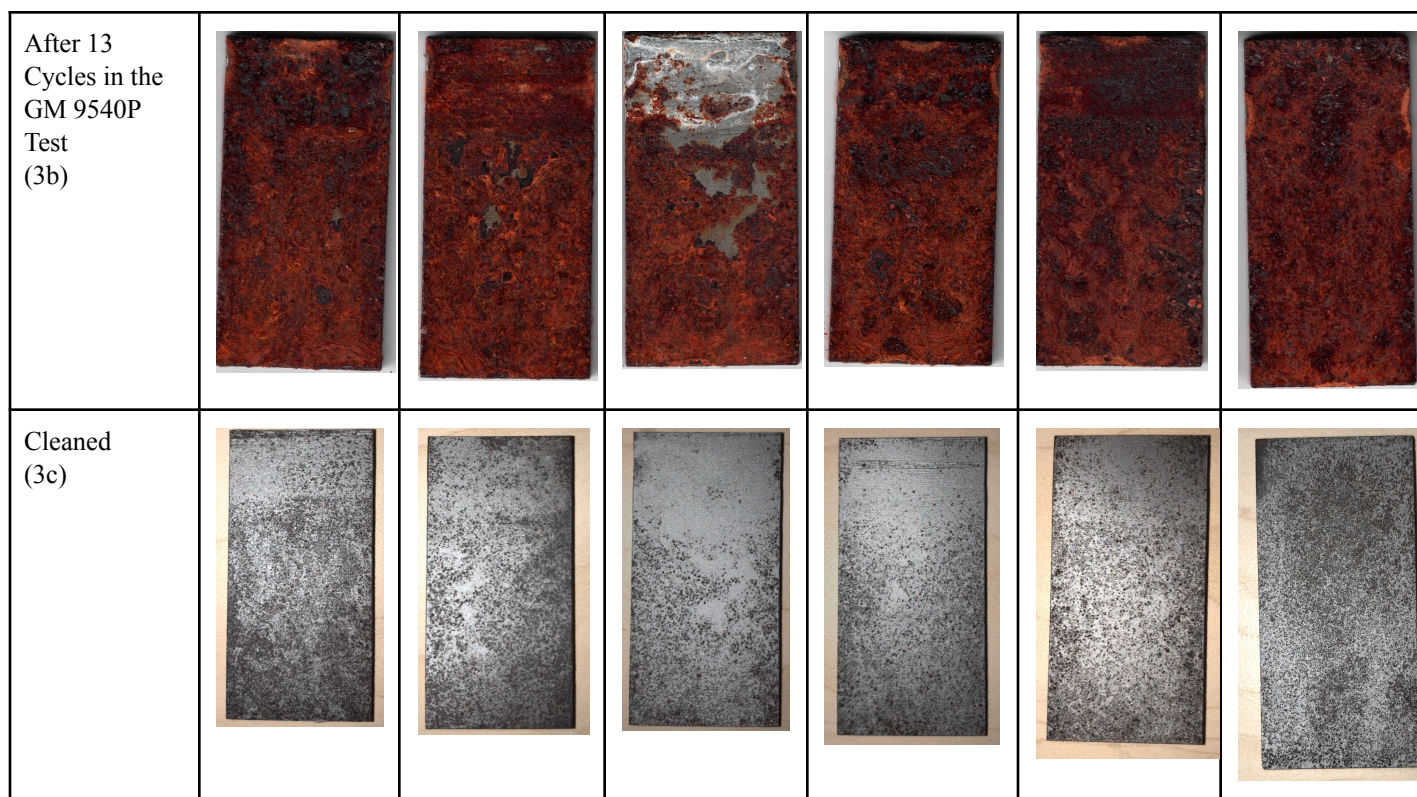


Figure 01: Representative 1018 Steel coupons partially coated with various aluminum alloys prior to exposure, after 13 cycles in the GM9540P accelerated corrosion test, and after cleaning.

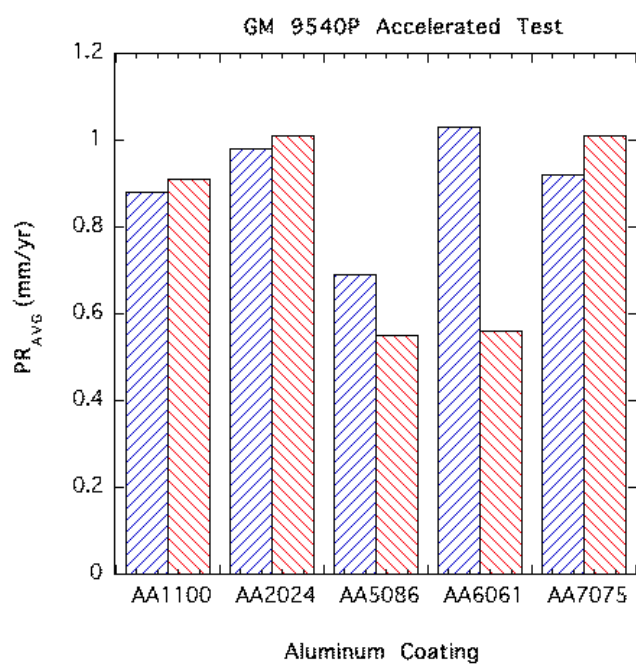


Figure 02: Average penetration rate of 1018 steel substrate (two specimens) based on specimen mass loss after all of the corrosion products and aluminum coating were removed. The original aluminum coating covered approximately a 1/2" x 1" strip on one side of the 1" x 2" x 1/8" samples. Both sides of the samples were exposed in the corrosion test.

Corrosion

The aluminum layer can serve as a barrier coating and sacrificial coating. In marine environments containing chlorides, the aluminum layer will cathodically protect the substrate 1018 steel. Less pitting can be seen in the region (Figure 1c) where the aluminum layer was deposited. Hence, the aluminum likely served as a barrier coating in the initial stages of exposure and then as a sacrificial coating as it was consumed. The cathodic “throwing power” of the aluminum coating can even be seen on some of the samples where the 1018 substrate was immune to corrosion even at a distance away from the original coating (1c). This was most noticeable for the AA5086 sample with the regions of thick aluminum deposits. The area fraction (Table??) of uncorroded aluminum was calculated for the samples in figure 1c.

AA1100	AA2024	AA5086	AA6061	AA7075	Blank
98.1%	96.9%	67.6%	99.3%	99.1%	99.4%

Table 07. Area fraction of surface corroded

Scanning Kelvin Probe (SKP) scans (Figure xa and xb) clearly show the demarcation between the aluminum coating and 1018 steel substrate on a typical virgin coated sample. After exposure to 13 cycles of the GM9540P test, the SKP scans (Figure xb) are virtually flat traversing the 1018 substrate and original aluminum coated regions, indicating that the aluminum layer beneath the corrosion products were totally consumed. Remnant aluminum coating was only sporadically found on a few samples.

SKP WF measurement has units of electron volts resolution of 1-3 meV

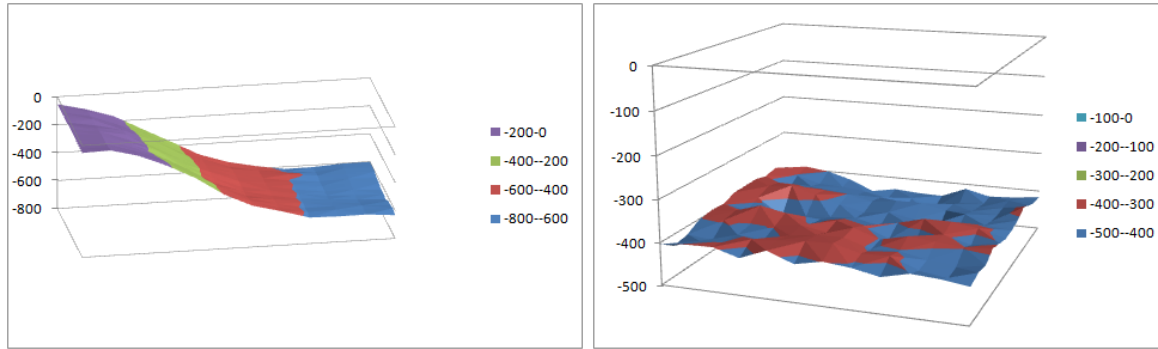


Figure xa. A) a typical plot of the work function (eV) of the boundary between aluminum and steel on a virgin AA1100 coated sample by scanning kelvin probe. B) a typical plot of the work function at the boundary between aluminum and steel on a corroded AA1100 coated sample.

A comparison of the corrosion rate of the substrate 1018 steel (Figure 02) showed that the best to worst protection was ordered as follows: AA5086, AA1100, AA6061, AA7075, AA2024. This ordering is consistent with the normal corrosion rates of the monolithic aluminum alloys. AA5085, AA1100, and AA6061 have significantly better corrosion resistance in marine environments compared to AA2024 and AA7075. The correlation is likely due to the slower normal corrosion rates of AA5085, AA1100, and AA6061 plus likely better adhesion and coverage compared to the AA2024 and AA7075 coatings. The AA2024 and AA7075 coatings had a significantly more textured appearance (Figure 1a) than those of the AA5085, AA1100, and AA6061, which is likely indicative of the adhesion integrity. Additionally AA2024 and AA7075 appeared to have the most discontinuous application onto the substrates. **The adhesion and coverage could possibly be related to the flow stress of the aluminum alloys.** The AA2024 and AA7075 are markedly stronger mechanically than the AA5085, AA1100, and AA6061. In these samples, consistent process parameters were used for all of the alloys and were not tailored to each. Hence, it is likely that the coating integrity for all of the alloys can be improved; however, the utilization of AA5086, AA1100, and AA6061 will likely be preferred due to their inherently better corrosion resistance, and apparent relative ease for deposition.

4. Conclusions

AA5086 offered the longest lasting corrosion protection, likely as a result of its greater deposition thickness. It is likely that if process parameters are optimized, AA1100 and AA6061 could also be viable coatings. The higher hardness and flow stress of AA2024 and AA7075 plus less inherent corrosion resistance make both of these alloys much less attractive as coatings.

Acknowledgments

We acknowledge the support from General Motors and NSF CMMI grant # 1763147.

References

1. Seidi, E., Miller, S. F., and Carlson, B. E., 2021, "Friction Surfacing Deposition by Consumable Tools." ASME. Journal of Manufacturing Science and Engineering, pp. 1-44. <https://doi.org/10.1115/1.4050924>
2. Sahoo, D. K., and Mohanty, B. S., 2019, "Evaluation of Bond Strength on Deposition of Aluminium 6063 Alloy over EN24 Medium Carbon Steel by Friction Surfacing Using Different Mechtrode Diameter," e-Journal of Surface Science and Nanotechnology, 17, pp. 83-94. <https://doi.org/10.1380/ejssnt.2019.83>
3. Gandra, J., Pereira, D., Miranda, R. M., and Vilaça, P., 2013, "Influence of process parameters in the friction surfacing of AA 6082-T6 over AA 2024-T3," Procedia CIRP, 7, pp. 341-346. <https://doi.org/10.1016/j.procir.2013.05.058>
4. Vasanth, R., Mohan, K., Rengarajan, S., Jayaprakash, R., and Kumar, R. A., 2019, "Characterization and corrosion effects of Friction surfaced IS-2062 E250 CU with AA6063," Materials Research Express, 6(12), 126579. <https://doi.org/10.1088/2053-1591/ab5981>
5. Kumar, B. V., Reddy, G. M., and Mohandas, T., 2015, "Influence of process parameters on physical dimensions of AA6063 aluminium alloy coating on mild steel in friction surfacing," Defence Technology, 11(3), pp. 275-281. <https://doi.org/10.1016/j.dt.2015.04.001>
6. Rafi, H. K., Ram, G. J., Phanikumar, G., and Rao, K. P., 2010, "Friction surfaced tool steel (H13) coatings on low carbon steel: A study on the effects of process parameters on coating characteristics and integrity," Surface and Coatings Technology, 205(1), pp. 232-242. <https://doi.org/10.1016/j.surfcoat.2010.06.052>
7. Guo, D., Kwok, C. T., & Chan, S. L. I., 2019, "Spindle speed in friction surfacing of 316L stainless steel—How it affects the microstructure, hardness and pitting corrosion resistance," Surface and Coatings Technology, 361, pp. 324-341. <https://doi.org/10.1016/j.surfcoat.2019.01.055>
8. Seidi, E., and Miller, S. F., 2019, "Friction Surfacing Using Consumable Tools: A Review," Proceedings of the ASME 2019 14th International Manufacturing Science and Engineering Conference. Volume 2: Processes; Materials, V002T03A048. <https://doi.org/10.1115/MSEC2019-2963>

9. Belei, C., Fitseva, V., Dos Santos, J. F., Alcântara, N. G., and Hanke, S., 2017, "TiC particle reinforced Ti-6Al-4V friction surfacing coatings," *Surface and Coatings Technology*, 329, pp. 163-173. <https://doi.org/10.1016/j.surfcoat.2017.09.050>
10. Guo, D., Kwok, C. T., and Chan, S. L. I., 2018, "Fabrication of stainless steel 316L/TiB₂ composite coating via friction surfacing," *Surface and Coatings Technology*, 350, pp. 936-948. <https://doi.org/10.1016/j.surfcoat.2018.03.065>
11. Oliveira, P. H. F., Galvis, J. C., Martins, J. D. P., and Carvalho, A. L. M., 2017, "Application of friction surfacing to the production of aluminum coatings reinforced with Al₂O₃ particles," *Materials Research*, 20, pp. 603-620. <https://doi.org/10.1590/1980-5373-mr-2017-0039>
12. Miranda, R. M., Santos, T. G., Gandra, J., Lopes, N., and Silva, R. J. C., 2013, "Reinforcement strategies for producing functionally graded materials by friction stir processing in aluminium alloys," *Journal of Materials Processing Technology*, 213(9), pp. 1609-1615. <https://doi.org/10.1016/j.jmatprotec.2013.03.022>
13. Karthik, G. M., Ram, G. J., and Kottada, R. S., 2016, "Friction deposition of titanium particle reinforced aluminum matrix composites," *Materials Science and Engineering, A*, 653, pp. 71-83. <https://doi.org/10.1016/j.msea.2015.12.005>
14. Seidi, E., and Miller S. F., 2020, "A Novel Approach to Friction Surfacing: Experimental Analysis of Deposition from Radial Surface of a Consumable Tool," *Coatings*, 10(11), 1016. <https://doi.org/10.3390/coatings10111016>
15. Seidi, E., and Miller, S. F., 2020, "Friction surfacing from radial surface of A6063 aluminum alloy consumable tool onto A36 carbon steel," *Proceedings of the ASME 2020 International Mechanical Engineering Congress and Exposition, Volume 2A: Advanced Manufacturing, Virtual, Online, V02AT02A003*. <https://doi.org/10.1115/IMECE2020-23502>
16. Khalid Rafi, H., Phanikumar, G. & Prasad Rao, K. Corrosion Resistance of Friction Surfaced AISI 304 Stainless Steel Coatings. *J. of Materi Eng and Perform* 22, 366–370 (2013). <https://doi.org/10.1007/s11665-012-0270-8>
17. Amit Kumar Singh, G. Madhusudhan Reddy, K. Srinivas Rao, Pitting corrosion resistance and bond strength of stainless steel overlay by friction surfacing on high strength low alloy steel, *Defence Technology*, Volume 11, Issue 3 2015, Pages 299-307, ISSN 2214-9147 <https://doi.org/10.1016/j.dt.2015.06.002>.
18. Mingrun Yu, Hongyun Zhao, Zili Zhang, Li Zhou, Xiaoguo Song, Ninshu Ma, Texture evolution and corrosion behavior of the AA6061 coating deposited by friction surfacing, *Journal of Materials Processing Technology*, Volume 291, 2021, 117005, ISSN 0924-0136, <https://doi.org/10.1016/j.jmatprotec.2020.117005>.

19. General Motors Corporation, "GM9540P Accelerated Corrosion Test," in General Motors Engineering Standards, Materials and Processes - Procedures, General Motors North America, December 1977, p. 1 - 9.
20. Ryan Sugamoto, George A. Hawthorn, and L.H. Hihara, "Comparison of Accelerated Corrosion Tests to Corrosion Performance in Natural Atmospheric Environments," 2009 DoD Corrosion Conference, Washington DC, August 2009.
21. MatWeb: Online Materials Information Resource, Accessed April 28, 2021, Available from: www.matweb.com